Second-generation Titanium alloys Ti-15Mo and Ti-13Nb-13Zr: A Comparison of the Mechanical Properties for Implant Applications

Florian Brunke, Carsten Siemers*, and Joachim Rösler

Technische Universität Braunschweig, Institut für Werkstoffe, Langer Kamp 8, 38106 Braunschweig, Germany

*c.siemers@tu-braunschweig.de

Abstract

Due to their outstanding mechanical properties, excellent corrosion resistance and biocompatibility titanium and titanium alloys are the first choice for medical engineering products. Alloys currently used for implant applications are Ti-6Al-4V (ELI) and Ti-6Al-7Nb. Both alloys belong to the class of (α+β)-alloys and contain aluminium as an alloying element. Aluminium is cytotoxic and can cause breast cancer. In addition, the stiffness of (α+β)-alloys is relatively high which can lead to stress shielding, bone degradation and implant loss. For this reason, second-generation titanium alloys like Ti-15Mo (solute-lean metastable β-alloy) and Ti-13Nb-13Zr (β-rich (α+β)-alloy) have been developed. However, their application in medical implants is limited due to a relatively low strength.

Therefore, in the present study, the mechanical properties of Ti-15Mo and Ti-13Nb-13Zr have been optimised by thermo-mechanical treatments to achieve high strengths combined with low stiffnesses. Different phase compositions have been used, namely, α-, β- and ω-phase in Ti-15Mo and α-, β- and α″-phase in Ti-13Nb-13Zr. For Ti-15Mo, the required mechanical properties' combination could not be achieved whereas Ti-13Nb-13Zr showed high strength and a low Young's modulus after a dedicated thermo-mechanical treatment. This makes the latter alloy a good option for replacing the (α+β)-alloys in implant applications in the future.

1. Introduction

In the recent years, the number of overweight people has increased and their health condition and fitness level has declined [1,2]. This leads to a higher wear of human bones and joints resulting in an increased demand of high-strength medical implants, especially in the western world. An opposite trend is visible as well as there is a large number of people carrying out extreme sports characterized by high speeds and high risks [3]. Consequently, younger people with excellent health condition need implants and osteosynthesis products as well.

Amongst all possible metallic materials titanium alloys fulfil the implants' requirements best. Therefore, α- or (α+β)-titanium alloys like CP-Titanium Grade 2 and 4, Ti-6Al-4V (ELI) and Ti-6Al-7Nb are used for osteosynthesis or implant applications for several decades now [4,5]. Although these alloys exhibit acceptable properties, some disadvantages exist: Vanadium as well as its oxides are cytotoxic [4]. Higher aluminium concentrations in the brain can lead to dementia. In addition, an intense discussion is driven if aluminium can cause breast cancer and the Alzheimer's disease [6–8]. Finally, the first-generation alloys exhibit a Young's modulus between 100 GPa and 120 GPa which is still up to five times higher than that of human long bones. Thus, stress shielding is observed leading to degradation of the bone and loosening of the implant up to implant loss [4,9].

Consequently, research of the last years concentrated on the introduction of titanium alloys into implant technology only containing non-critical alloying elements like molybdenum, niobium, zirconium, iron and silicon. In these so-called second-generation implant alloys like Ti-13Nb-13Zr (β-rich α+β alloy) and Ti-15Mo (solute-lean metastable β-alloy) unfavourable alloying elements were avoided and the stiffness is comparably low [10]. In addition, these alloys offer a large flexibility to enhance their strength as they can be precipitation hardened by fine-dispersed α-phase. Phase transformations leading to the formation of metastable phases like α″ or ω are possible as well. Unfortunately, implant manufacturing by machining is extremely difficult [11–13].

In the present study, the mechanical properties of Ti-15Mo and Ti-13Nb-13Zr were systematically varied (and optimised) by different thermo-mechanical treatments. As a general aim, an ultimate tensile strength of 930 N/mm² at an elongation at rupture of 10% (requirements of ASTM F1472) at the lowest possible Young's modulus should be achieved. The microstructure, the phase composition and the resulting mechanical properties were investigated.

2. Materials and Experiments

Alloy and sample production

Ti-15Mo used in our experiments has been produced by the GfE GmbH in Nuremberg, Germany. The electron-beam melted and cast ingot has been deformed by rotary swaging to a final diameter of approx. 80 mm. Out of this bar, samples of about 10 mm x 10 mm x 10 mm have been cut. To gain a single β-phase microstructure, all samples have been solution treated

(ST) at 800°C in the single β-phase field for 30 minutes and were afterwards water quenched (WQ). In addition, possible residual stresses from the deformation process were removed and equal starting conditions for all samples were ensured. Afterwards, heat treatments at elevated temperatures (225°C – 700°C) at holding times between 5 minutes and 360 hours followed by air cooling (AC) have been performed to precipitate ω- and α-phase in the matrix. All heat treatments have been carried out in air.

Ti-13Nb-13Zr alloy has been produced by the GfE as well and was remolten (VAR skull melting) by ARCONIC Power and Propulsion TITAL GmbH in Bestwig, Germany, followed by investment casting. The cast bars had a width between 17 mm and 19 mm, a height between 11 mm and 13 mm and a maximum length of 150 mm. The bars were hot-rolled at approx. 650°C (degree of deformation of $\varphi \approx 1$). Out of the rolled material, samples with a cross section of approx. 4 mm x 20 mm have been cut. Afterwards, heat treatments have been carried out to recrystallise the material and to produce different microstructures (globular, lamellar etc.). These microstructures were precipitation hardened in a standard air-furnace between 300°C and 500°C in a second step using holding times between 1 hour and 24 hours.

Metallographic sample preparation and microstructure analysis

For metallographic analyses, samples were embedded (approx. 180°C / 200bar) into fibre-reinforced polymers and cross-sections were prepared by grinding with SiC paper starting at grain size P180 to a final grain size of P2500 [10]. After grinding, the samples were polished with a diamond suspension (9 µm, 6 µm, 3 µm). The final polishing of Ti-15Mo was performed in several cycles with a mixture of OPS (50 ml) and H_2O_2 (10 ml). Between and after the final polishing steps, the samples were etched with Kroll's reagent (3 ml HF, 6 ml HNO_3, 100 ml H_2O) or a special etching reagent (5 ml HF, 5 ml HNO_3, 86 ml H_2O, 12 ml H_2O_2) developed for metastable β-titanium alloys. Ti-13Nb-13Zr was polished with a mixture of OPS (25 ml), H_2O (10 ml) and KOH (0.7 g). The etching solution consisted of 10 ml HF, 60 ml H_2O_2 and 30 ml H_2O.

The microstructure of the samples was analysed by a Zeiss Imager.M2m optical microscope and by a Leo Gemini 1550 scanning electron microscope using an In-lens detector. Furthermore, the embedded samples were coated with a thin Gold layer to allow high resolution SEM imaging.

Phase analyses

Phase analyses were performed using hard X-rays at P07 of PETRA III, DESY (in two different beamtimes). Samples were investigated in transmission (Debeye-Scherrer configuration) and the resulting diffraction patterns were recorded by a Perkin Elmer XRD 1621 flat panel detector [14]. The energy of the beam was chosen to 84.8 keV (98.5 keV) leading to a wavelength of $\lambda = 0.01462$ nm ($\lambda = 0.012587$ nm). The samples were exposed to the beam for 0.5 seconds. Fifteen frames were averaged to achieve the final XRD patterns for each measurement; five points (area of exposure 0.5 mm x 0.5 mm) were investigated for each sample. The diffraction patterns were ring integrated (2θ angle) using the fit2D software [15]. Afterwards the CMPR Logic software [16] was used together with a PDF 2 database (release 2005) to calculate and identify the peak positions of β-, α-, α″- and ω-phases as well as additional phases.

Mechanical Properties

The static mechanical properties were determined by automated Vickers hardness measurements (HV10) at the metallographic cross-sections. In addition, tensile tests were performed according to DIN EN ISO 6892 1:2009. The tensile test samples of Ti-15Mo were produced according to DIN 50125-B 5x25. In terms of the rolled Ti-13Nb-13Zr alloy, flat tensile test specimens were used.

3. Results and Discussion

Ti-15Mo alloy

In the solution treated state (ST), the microstructure consisted of equiaxed β grains with an average grain size of approx. 200 µm and an average hardness of 227 HV10. As reported before for metastable β-alloys, ω-phase already precipitated stress induced (athermally) during quenching [17,18]. The phase analyses showed strong β- and weak ω-peaks which are characteristic for nano-crystalline precipitations (see Figure 1 (a)) [10]. Aging treatments between 225°C and 700°C were performed to study the ω- and α-phase precipitation in the β matrix.

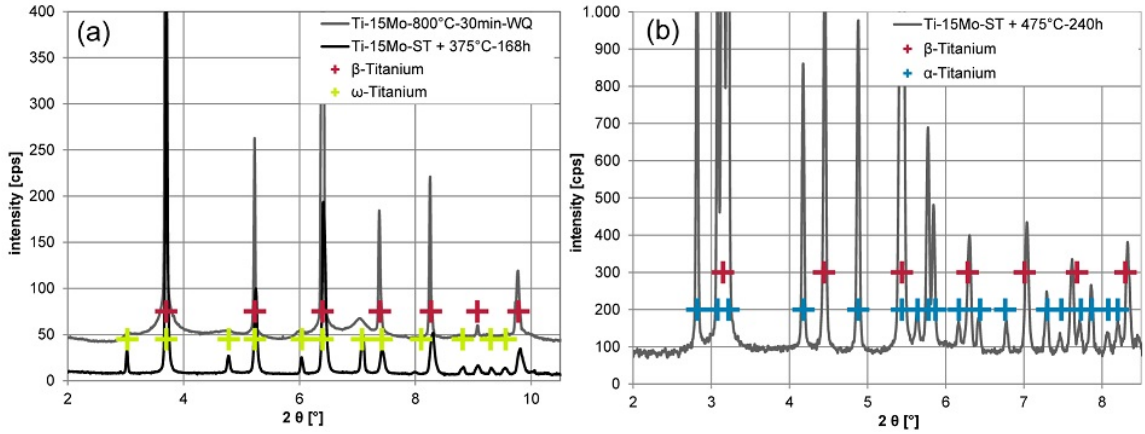

Figure 1: Phase analyses of Ti-15Mo alloy: In the solution treated state β-phase and nano-sized ω-phase is present (a). In the aged state (375°C for 168 hours), the ω-peaks are well pronounced (indicating particle growth and volume increase). After a heat treatment at 475°C for 240 hours only β- and α-phase were present (b).

At 225°C, an increase in hardness was observed after 15 minutes whereas the samples annealed at higher temperatures (≥ 250°C) already showed higher hardnesses after 5 minutes of exposure time. In the diffraction patterns, a sharpening of the ω-peaks (indicating a growth of the ω-precipitations) from 5 minutes to 360 hours was observed. Moreover, the height difference between the β-and the ω-peaks was diminished, which could be laid back to a higher ω-volume fraction. The maximum hardness (500 HV10) was reached after annealing at 350°C for 120 hours. As expected, the precipitation of larger quantities of ω-phase led to an increased embrittlement. In related tensile tests a total absence of plastic deformation (elongation at rupture 0 %, see Figure 2, left) was observed.

During the heat treatments at 425°C (450°C and 475°C) a (partial) phase transformation from ω- to α-phase occurred after 240 hours (96 h and 16 h). After 240 hours at 475°C, only β- and fine dispersed α-phase were present (see Figure 1 (b)). Due to the phase transformation (ω→α), the strength decreased significantly and the elongation at rupture increased. Both ω- and α-phase led to an increase of the Young's modulus, whereas the effect of the ω-phase was much stronger. Heat treatments at higher temperature (e. g. 550°C) with a holding time of a few hours led to the precipitation of elongated needle-like α-phase and ω-phase during air cooling. The α-phase coarsened with longer holding times. Figure 2 shows the effect of β-, α- and ω-phase on the resulting mechanical properties. None of the performed heat treatments resulted in a combination of high strength, low stiffness and sufficient ductility as required for Ti-6Al-4V in ASTM F 1472.

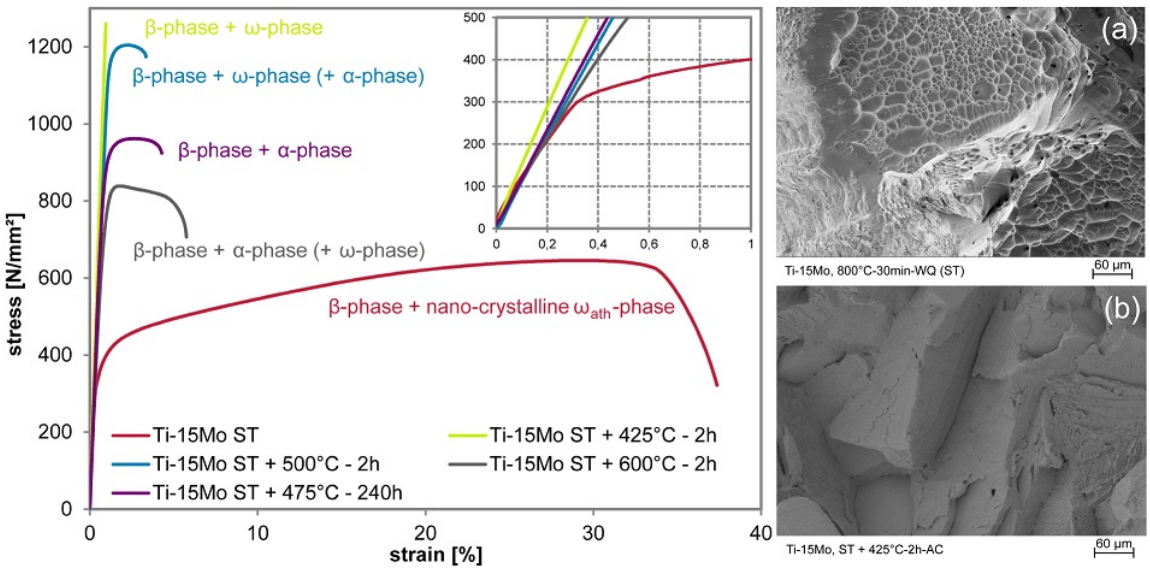

Figure 2: Stress-strain curves of Ti-15Mo alloy in different states. ω- and α-phase increased the strength and the stiffness whereas the ductility was decreased (left). Increased amounts of ω-phase changed the fracture mechanism from a ductile dimple fracture (a) to a brittle fracture (b).

Ti-13Nb-13Zr alloy

In a first study, for Ti-13Nb-13Zr, heat treatments at ≥ 750°C were carried out without prior deformation followed by different cooling procedures including holding steps. (1) During a heat treatment at 800°C (above $T_{\beta,}$ T_{β} ≈ 735°C [19]) a β-phase microstructure was produced which transformed martensitically after fast cooling. As the martensite showed a comparably low hardness of 230 HV10, a low stiffness of approx. 60 GPa and good formability, it is concluded that the orthorhombic α″-martensite formed during quenching. (2) Slow (furnace) cooling from 800°C to 700°C with a holding time of 4 hours followed by water quenching led to a composition of α- and α″-phase (see Figure 3 (a)). (3) Cooling to 625°C with a holding time of 8 hours followed by water quenching resulted in a composition of α-phase and a maximum amount of (metastable) β-phase stabilised to room temperature by the element partitioning effect (see Figure 3 (b)). Both phases, the α″- and the metastable β-phase, could be precipitation hardened in a second step.

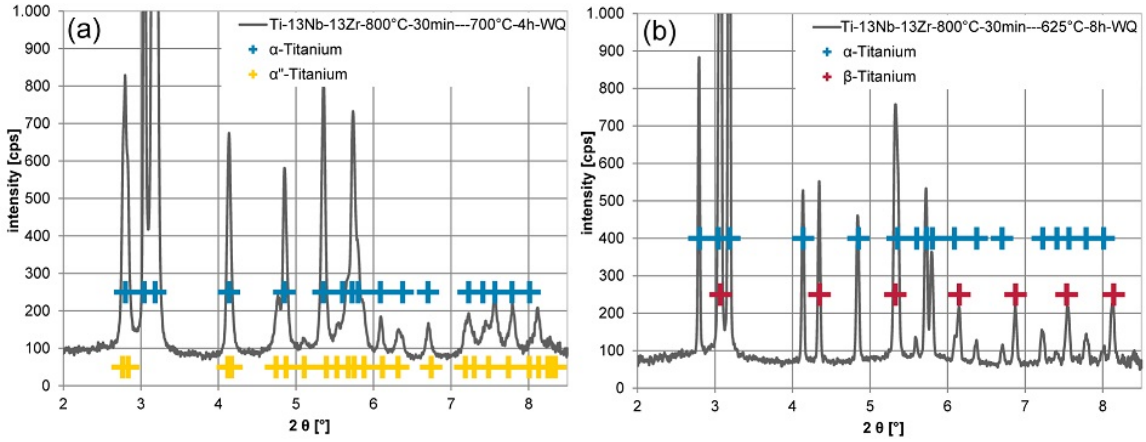

Figure 3: Phase analysis of Ti-13Nb-13Zr: After a solution treatment at 800°C, the alloy was slow cooled to 700°C or 625°C, respectively. (a) A holding time of 4 hours at 700°C and WQ led to a α_p/α''-microstructure. (b) An 8-hour heat treatment at 625°C led to an enrichment of Nb in the β-phase. After WQ, the alloy consisted of α_p- and metastable β-phase.

Secondly, the material was hot-rolled and a large study was performed in which the temperature and holding times were varied to investigate the recrystallisation behaviour. To obtain optimised microstructures and mechanical properties being acceptable for implant applications, the rolled material was recrystallised in two different ways (only the optimal process parameters are presented here) to produce the phase compositions described before. (1) Recrystallisation at 700°C was performed to produce fine α_p-grains and recrystallised β-grains. After 4 hours, the material was water quenched ensuring that the β-phase transformed to α″ (α_p/α''), see Figure 4 (b). The hardness of this microstructure was measured to 215 HV10. The following ageing treatment, i.e. a partial martensite decomposition, at 475°C for 8 hours led to an increased hardness of approx. 300 HV10 (α_p/α'' aged). (2) Recrystallisation was carried at 675°C for 6 hours; afterwards the material was slow cooled to 625°C and held for 8 hours followed by water quenching. The resulting microstructure consisted of globular α_p-grains (≈ 5 µm) and metastable, niobium-enriched β-phase ($\alpha+\beta_{ms}$, hardness of 218 HV10), see Figure 4 (a). Finally, increased hardness of 300 HV10 was achieved through precipitation (350°C for 8 hours) of fine dispersed α- in the β-phase (α+β aged).

Tensile tests of the α_p/α''-microstructure showed a UTS of 730 N/mm² and an elongation at rupture of 18 %; the globular ($\alpha+\beta_{ms}$)-microstructure had a UTS of 670 N/mm² at 20 % elongation. The Young's modulus was determined to less than 60 GPa for both microstructures. Ageing increased the ultimate strength as expected, but due to the presence of additional α-phase, the stiffness increased as well, see Figure 4, left: (α+β aged) microstructure: R_m = 900 N/mm², A = 9 % and E = 84 GPa; (α_p/α'' + aged): R_m = 1020 N/mm², A = 8,5 %, E = 80 GPa In the aged state, both microstructures showed a sufficient strength for an implant application but forfeited part of their advantage of a comparably low Young's modulus, even if it remained about 30 GPa beneath the Young's modulus of Ti-6Al-4V. Without the precipitation hardening, the Young' modulus was pleasingly low, but the strength was too low as well.

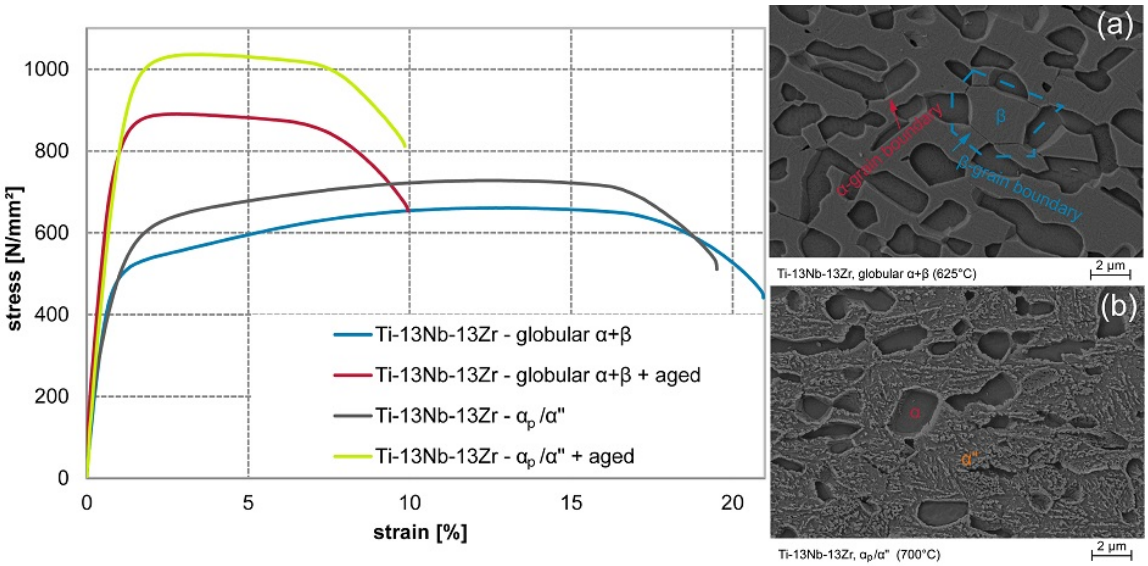

Figure 4: Stress-strain curves of Ti-13Nb-13Zr alloy in different states (left). The globular α+β_{ms} (a) and the α_p/α'' (b) microstructure showed good ductility and low stiffness. An ageing heat treatment led to increased strength and stiffness.

4. Conclusions and outlook

Starting with a recrystallised and solution treated Ti-15Mo alloy, heat treatments did not lead to microstructures with well-balanced mechanical properties. While previous work has shown promising results for Ti-15Mo with low ω-volume content [10], ω-phase in higher amounts led to a strong embrittlement. Although the brittleness decreased with (partial) transformation of ω- to α-phase, the combination of strength and elongation was poor and did not reach the values requested for Ti-6Al-4V.

In contrast to this, the β-rich (α+β)-alloy Ti-13Nb-13Zr showed promising results. Microstructures with a large volume fraction of either α″ or β exposed a comparably low Young's modulus (< 60 GPa) as desired for the stem of a hip implant. The stem is in direct contact with the bone and ensures force transfer to it. A high stiffness difference between bone and implant usually causes bone loss. The non-aged microstructures presented here could have a clear advantage compared to the two standard alloys. The strength of Ti-13Nb-13Zr in the solution-treated and water-quenched state might additionally be increased by a finer microstructure, which could be achieved by severe plastic deformation followed by recrystallisation. To absorb the high forces in the neck and neck-shoulder junction of a hip implant, an additional local heat treatment could be carried out in this area, for example, by inductive heating. Initial tests have already been carried out and have shown that the hardness can be increased without damaging the surface (no α-case or oxide growth occurred due to the relatively low temperatures applied). Therefore, it is feasible that implants of Ti-13Nb-13Zr with graded properties might be produced. Future work will therefore concentrate on testing real implants of Ti-13Nb-13Zr with designed graded properties (according to ISO 7206).

Even without graded properties, Ti-13Nb-13Zr alloy in both aged states presented here outnumber the mechanical properties' combination of Ti-6Al-4V alloy. In addition, Ti-13Nb-13Zr has a better biocompatibility and no critical elements are used. This might make Ti-13Nb-13Zr a good choice as a future implant material.

5. Acknowledgements

The research leading to the results presented here has been funded by the Arbeitsgemeinschaft industrieller Forschungsvereinigungen (AiF), project number IGF 16841 and IGF 18116. Financial support is therefore gratefully acknowledged. The research study was supported by hard X-ray experiments at PETRA III, beamline P07, DESY.

6. References

[1] K.M. Flegal, M.D. Carroll, C.L. Ogden, C.L. Johnson, 1999-2000, JAMA 288 (2002) 1723–1727.
[2] R.J. Kuczmarski, K.M. Flegal, S.M. Campbell, C.L. Johnson, JAMA 272 (1994) 205–211.
[3] E. Brymer, Annals of Leisure Research 13 (2010) 218–238.
[4] M. Geetha, A.K. Singh, R. Asokamani, A.K. Gogia, Progress in Materials Science 54 (2009) 397–425.
[5] C. Leyens, M. Peters (Eds.), Titanium and Titanium Alloys: Fundamentals and applications, Wiley-VCH, Weinheim, 2005.
[6] N.D. Priest, Journal of environmental monitoring JEM 6 (2004) 375–403.
[7] K. Nagasawa, S. Ito, T. Kakuda, K. Nagai, I. Tamai, A. Tsuji, S. Fujimoto, Toxicology letters 155 (2005) 289–296.
[8] R.A. Yokel, D.D. Allen, D.C. Ackley, Journal of Inorganic Biochemistry 76 (1999) 127–132.
[9] A.G. Robling, A.B. Castillo, C.H. Turner, Annual review of biomedical engineering 8 (2006) 455–498.
[10] F. Brunke, C. Siemers, J. Rösler, in: V. Venkatesh, A.L. Pilchak, J.E. Allison, S. Ankem, R.R. Boyer, J. Ch (Eds.), 2015 World Conference on Titanium, 1st ed., Wiley-TMS, 2016, 929–934.

[11] W. Ho, Journal of Medical and Biological Engineering 28 (2008) 47.
[12] M.J. Donachie, Titanium: A technical guide, 2nd ed., ASM International, Materials Park, OH, 2000.
[13] A.W. Bowen, J Mater Sci 12 (1977) 1355–1360.
[14] N. Schell, A. King, F. Beckmann, T. Fischer, M. Müller, A. Schreyer, MSF 772 (2013) 57–61.
[15] A.P. Hammersley, S.O. Svensson, M. Hanfland, A.N. Fitch, D. Hausermann, High Pressure Research 14 (1996) 235–248.
[16] B.H. Toby, J Appl Crystallogr 38 (2005) 1040–1041.
[17] J.L. Murray, Bulletin of Alloy Phase Diagrams 2 (1981) 185–192.
[18] G. Lütjering, J.C. Williams, Titanium, 2nd ed., Springer-Verlag, Berlin, Heidelberg, 2007.
[19] A.K. Mishra, J.A. Davidson, R.A. Poggie, P. Kovacs, T.J. FitzGerald, in: S.A. Brown, J.E. Lemons (Eds.), Medical Applications of Titanium and Its Alloys: The Material and Biological Issues, ASTM International, West Conshohocken, PA 19428-2959, 1996, 96-112.